

ChemComm

Chemical Communications

Accepted Manuscript

This article can be cited before page numbers have been issued, to do this please use: M. Francis, A. Patra, F. A. Salam, L. Ungur, B. Schwarz and S. Roy, *Chem. Commun.*, 2025, DOI: 10.1039/D4CC06550F.



This is an Accepted Manuscript, which has been through the Royal Society of Chemistry peer review process and has been accepted for publication.

Accepted Manuscripts are published online shortly after acceptance, before technical editing, formatting and proof reading. Using this free service, authors can make their results available to the community, in citable form, before we publish the edited article. We will replace this Accepted Manuscript with the edited and formatted Advance Article as soon as it is available.

You can find more information about Accepted Manuscripts in the [Information for Authors](#).

Please note that technical editing may introduce minor changes to the text and/or graphics, which may alter content. The journal's standard [Terms & Conditions](#) and the [Ethical guidelines](#) still apply. In no event shall the Royal Society of Chemistry be held responsible for any errors or omissions in this Accepted Manuscript or any consequences arising from the use of any information it contains.

COMMUNICATION

Isolation and Oxygen Activation of Electron-Rich Co^{II}₄O Metallic Clusters Having a 3-Fold SymmetryMaria Francis,^a Asutosh Patra,^a Farsana Abdul Salam,^a Liviu Ungur,^b Björn Schwarz,^{*c} and Sudipta Roy^{*a}Received 00th January 20xx,
Accepted 00th January 20xx

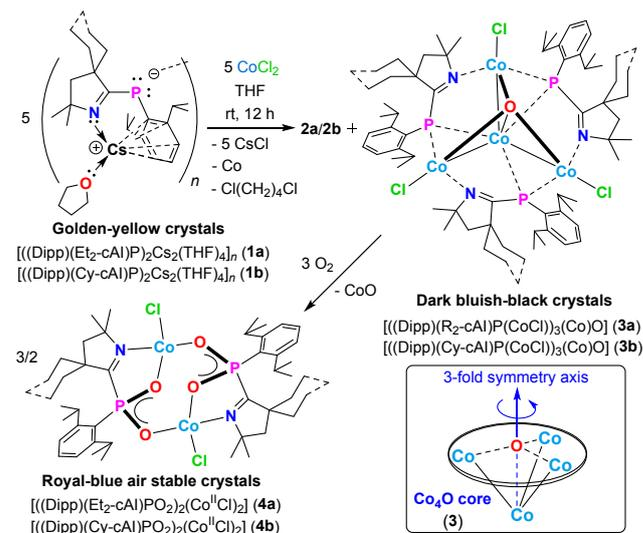
DOI: 10.1039/x0xx00000x

Two novel atomically precise tetra-nuclear cobalt clusters (3a-3b) having Co^{II}₄O core with 3-fold symmetry, and three short Co-Co distances of 2.7046(4) Å are isolated with three chelating NP-donor mono-anionic ligands. 3a-3b are shown to react with O₂, producing dinuclear cobalt complexes (4a-4b), where the P-centres of the ligands are oxygenated. All complexes are structurally characterized by single-crystal X-ray diffraction, and further studied by UV-vis, IR spectroscopy, CV, magnetic susceptibility measurements, and DFT calculations.

Metallic cobalt-clusters [Co_n/Co_nO] are known to exhibit numerous applications. Cobalt-carbonyls and their polynuclear analogues (Co₄, Co₁₀, etc.) have attracted chemists for their structural aspects, bonding, and unusually higher stability.¹ Co₂(CO)₈ is known for hydroformylation of olefins.¹ The stability, and bonding of metallic Co_n clusters (n = 4, 13) on the graphene surface have been studied by DFT calculation.² Co₁₃ cluster is known to absorb CO gas.^{2d} Co₄ coordination cluster is found to be effective in boosting the oxygen reduction of Fe–N–C catalysts with single-atom Fe–N₄ configurations.³ Adsorption of H₂ on cobalt clusters Co₆, Co₁₃ has been studied by DFT calculations.⁴ Hydrocarbon-soluble Co₄ nano-catalyst having spin crossover property⁵ is known to display excellent catalytic hydrogenation of unsaturated hydrocarbons at low temperature/pressure,⁶ while the corresponding cation exhibited slow relaxation of magnetization having S = 9/2 spin ground state.⁵ Co₄ cluster on graphdiyne surface acts as a catalyst for electro-chemical N₂ reduction producing ammonia.⁷ Co_n^{2a-c, 8a-b} (n = 4, 6, 13), and Co_nO^{8c-d} clusters (n = 2, 3, 11) have been deposited on surfaces, followed by utilization in hydrogenation, and oxygenation reactions.⁸ Decomposition of N₂O/NO on Co_n clusters have been

theoretically investigated.⁹ Co-clusters confined in mesoporous silica nanospheres containing N-doped carbon have been shown to efficiently dissociate O–O bond of peroxymonosulphate, producing HO[•], and SO₄^{•-} radicals.¹⁰ The sub-nanocluster Co₄-catalysts deposited on silanol nests containing both ionic Co–O, and metallic Co–Co bonds are known for efficient dehydrogenation of propane.¹¹ Herein, we report on the solid-state isolation of highly air, and moisture-sensitive structurally well-defined organic solvent-soluble tetranuclear Co^{II}₄O metal-clusters **3a-3b**, and the corresponding oxygen-activated dimeric Co^{II}₂ complexes **4a-4b**.

A 1:2 molar mixture of the orange crystals of Cs-(Dipp)-cyclic alkyl(imino) phosphide (**1a**),¹² and anhydrous CoCl₂ was stirred in THF at rt for 12 h under an argon atmosphere. Upon filtration, the insoluble black precipitate was separated, and the concentrated dark bluish-black filtrate was stored at -40 °C in a freezer. After 3-4 weeks, dark bluish-black hexagonal crystals of [((Dipp)(Et₂-cAl)P(CoCl))₃(Co)O] (**3a**) were obtained in 35% yield (**Scheme 1**).



Scheme 1. Syntheses of Co^{II}₄O clusters **3a-3b** [Co1–Co2 2.7046(4)], and their reactivity with O₂ affording dimeric Co^{II}₂ complexes **4a-4b**. **2a-2b** are the respective bis-(Dipp)(imino)-phosphine by-products, isolated separately as white needles (see ESI).

^a Department of Chemistry, Indian Institute of Science Education and Research (IISER) Tirupati, Tirupati – 517619, India. Email: roy.sudipta@iisertirupati.ac.in

^b Department of Chemistry, National University of Singapore, Singapore.

^c Institute for Applied Materials (IAM), Karlsruhe Institute of Technology (KIT), Hermann-von-Helmholtz-Platz 1, Karlsruhe, D-76344, Germany. Email: bjoern.schwarz@kit.edu

Electronic Supplementary Information (ESI) available. CCDC: 2324725 (**2a**), 2324727 (**3a**), 2324726 (**4a**), 2344451 (**2b**), 2344452 (**4b**). For ESI and crystallographic data in CIF or another electronic format see DOI: 10.1039/x0xx00000x



Colorless, manually separable needles of bis-(Dipp)(imino)-phosphene (**2a**) were produced after 2-3 days as the by-product in 29% of isolated yield. When a similar reaction mixture as stated above with 1:2 molar ratio of **1a** and anhydrous CoCl_2 , following the 12 h of stirring at rt was exposed to air for 15 min, the bright blue blocks of the oxygen activated dimeric Co^{II} complex $[\text{((Dipp)(Et}_2\text{-cAl)PO}_2)_2(\text{Co}^{\text{II}}\text{Cl})_2]$ (**4a**) was isolated in 30% yield after 2-3 days of storing the concentrated reaction mixture at -40°C in a freezer (Scheme 1). When a 1:2 molar ratio of **1b**, and anhydrous CoCl_2 in THF at rt afforded highly crystalline tetranuclear Co^{II} metal cluster $[\text{((Dipp)(Cy-cAl)P}(\text{CoCl})_3(\text{CoO}))]$ (**3b**) in 39% of isolated yield (Scheme 1). Several attempts were failed to produce the good quality single crystals of **3b**, suitable for X-ray diffraction. Exposure of the above-mentioned reaction mixture to air afforded the air-stable royal blue blocks of the Co^{II} complex $[\text{((Dipp)(Cy-cAl)PO}_2)_2(\text{Co}^{\text{II}}\text{Cl})_2]$ (**4b**) from a freezer at -40°C in 30% yield. The purity of the isolated crystals of **3a-3b**, and **4a-4b** have been confirmed by the elemental analyses (see ESI).

The Co^{II} clusters **3a-3b** were highly air and moisture-sensitive. **3a-3b** were highly soluble in polar solvents, such as THF and DCM. The crystalline solids, and THF and/or DCM solutions of **3a-3b** were stable at rt under argon atmosphere for more than 6 months. The powders of **3a-3b** were melted to yellow liquids at 209-210, and 211-212 $^\circ\text{C}$, respectively. The dimeric Co^{II} complexes **4a-4b** were air stable for a week, and sparingly soluble in THF. The powder of **4a-4b** were melted to yellow liquids under an argon atmosphere at 175-177, and 174-176 $^\circ\text{C}$, respectively.

3a-3b have been characterized by IR, and UV-vis spectroscopy (see ESI). The UV-Vis absorption spectrum of the DCM solution of **3a** showed broad absorption bands with the corresponding maxima at 596 nm, and 597 nm with molar absorption coefficient (ϵ) values of 4862.38 and 229.35 $\text{M}^{-1}\text{cm}^{-1}$, respectively. Whereas, **4a** exhibited the absorption maxima at 289, 589, 657 nm with ϵ values of 3283.01, 113.20, and 273.58 $\text{M}^{-1}\text{cm}^{-1}$, respectively (see ESI). The computed $\text{IR}_{\text{p-o}}$ stretching frequencies for the PO_2^- moiety in the model complex **4b'** were found to be 1067.16 cm^{-1} , and 1213.93 cm^{-1} for the symmetric and asymmetric modes, respectively, which were comparable with the experimental $\text{IR}_{\text{p-o}}$ stretching frequencies observed for **4a-4b** (1070, 1210 cm^{-1} for **4a**; 1084, 1259 cm^{-1} for **4b**). These frequencies can be well compared with the reported stretching frequencies observed in $\text{L}:(\text{O})_2\text{P}-\text{P}(\text{O})_2:\text{L}$ ($\text{L} = \text{:C}\{\text{N}(2,6\text{-Pr}^i_2\text{C}_6\text{H}_3)\text{CH}\}_2$) (1279 cm^{-1} , 1061 cm^{-1}),¹³ $[(\text{PO}_2)\{\text{Re}(\text{PyrPz})(\text{PNP})\}]$ (1263 cm^{-1} , 1086 cm^{-1}),¹⁴ and the reported data for the free PO_2^- anion in a KCl matrix (1097 cm^{-1} , 1207 cm^{-1}).¹⁵

3a, 4a-4b have been structurally characterized by single-crystal X-ray diffraction (Figures 1-2, see ESI). **3a** crystallizes in the trigonal $R3c$ space group with a 3-fold rotational axis of symmetry passing through the $\text{Co}2\text{-O}1$ bond (2.036(2) Å) (Figure 1). The structural feature of **3a** can be correlated with a stemless mushroom possessing three Co^{II} ions (three Co^{I} centres; Co-O distance of 1.9589(3) Å) in the periphery and

a Co^{II} centre ($\text{Co}2$) at the top. All the four Co^{II} atoms are connected through the $\mu_4\text{-O}$ atom, which lies 0.16 Å above the plane of the three peripheral Co^{I} ions ($\text{Co}1$), whereas, the central $\text{Co}2$ atom is 1.87 Å below this plane. $\text{Co}2$ atom is also 0.09 Å away from the plane containing three P1 atoms of the three (Dipp)-cyclic alkyl(imino) phosphide $[(\text{Dipp})(\text{cAl})\text{P}^-]$ ligands. The $\text{Co}1\text{-Co}2$ distance in **3a** is found to be 2.7046(3) Å, which is significantly longer than that of the Co-Co distances present in the previously reported complexes $[(\text{IME}_4)_2\text{M}(\mu\text{-PMes})_2]$ ($\text{M} = \text{Co}$) (2.5241(9) Å),¹⁶ and triply $\mu\text{-O}_{\text{alkoxy}}$ bridged Co^{III} -complex $[\text{Co}^{\text{III}}_2(\text{hep})_3(\text{N}_3)_3]\cdot\text{DMF}$ (2.595(6) Å),¹⁷ but slightly longer than that of $(\text{Me}_2\text{-cAAC})_2\text{Co}_2$ (2.6550(6) Å).¹⁸ $\text{Co}1\text{-P}1$, and $\text{Co}2\text{-P}1$ bond distances in **3a** are found to be 2.4171(5) Å, and 2.2808(4) Å, respectively, in which the former one is comparable with that of the previously reported $[\text{Co}\{\text{PH}(\text{IDipp})\}\{\text{N}(\text{SiMe}_3)_2\}_2]$ complex (2.4572(8) Å).¹⁹

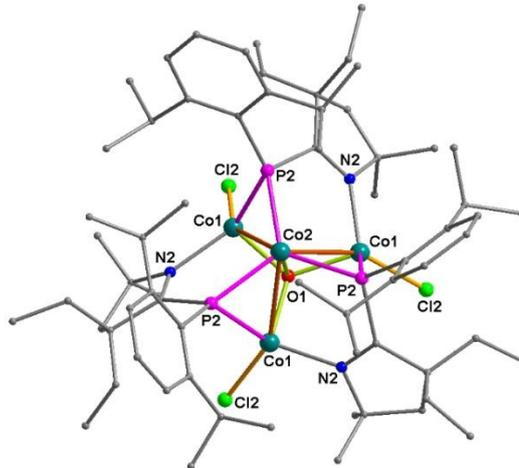


Figure 1. Molecular structure of Co_4 metal cluster $[\text{((Dipp)(Et}_2\text{-cAl)P}(\text{CoCl})_3(\text{CoO}))]$ (**3a**). Hydrogen atoms are omitted for clarity. Important bond lengths [Å], and bond angles [$^\circ$]: $\text{Co}1\text{-Co}2$ 2.7046(4), $\text{Co}1\text{-O}1$ 1.9589(3), $\text{Co}1\text{-Cl}1$ 2.2395(5), $\text{Co}2\text{-O}1$ 2.036(2), $\text{Co}2\text{-P}1$ 2.2808(4), $\text{P}1\text{-C}10$ 1.8397(17); $\text{C}10\text{-P}1\text{-Co}2$ 113.94(6), $\text{C}10\text{-N}1\text{-Co}1$ 127.76(12). Three-fold axis is present along $\text{Co}2\text{-O}1$ bond.

The $\text{P}1\text{-C}10$ bond distance in **3a** is found to be 1.8397(17) Å, which is typical of a P-C single bond. The $\text{N}1\text{-C}10$ bond length in complex **3a** is found to be 1.296(2) Å, which is comparable to that of complex **1a** (1.301(3) Å).¹²

The molecular structure of **4a** has been depicted in Figure 2 (see ESI for **4b**).

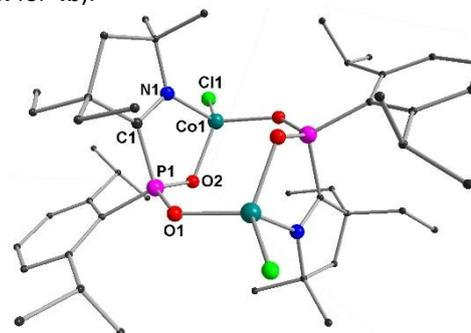


Figure 2. Molecular structure of $[\text{((Dipp)(Et}_2\text{-cAl)PO}_2)_2(\text{Co}^{\text{II}}\text{Cl})_2]$ (**4a**). Hydrogen atoms are omitted for clarity. $\text{Co}2$ and $\text{O}1$ have 0.33 occupancy each. The ethyl group ($\text{C}9\text{C}10$) is disordered with a site occupancy ratio of 53:47. Important bond lengths [Å], and bond angles [$^\circ$]: $\text{Co}1\text{-Cl}1$ 2.2034(11) [2.204], $\text{Co}1\text{-O}1$ 1.941(2) [1.933], $\text{Co}1\text{-}$



N1 2.042(3) [1.912], P1—O2 1.512(3) [1.554], P1—O1 1.514(3) [1.539], P1—C1 1.843(4) [1.824], N1—C1 1.282(5) [1.296]; O2—P1—O1 113.39(15) [114.96], P1—O2—Co1 115.66(15) [116.31].

4a crystallized in the monoclinic space group $P2_1/n$. The asymmetric unit of **4a** is composed of the monomeric unit $[(\text{Dipp})(\text{cAl})\text{PO}_2]\text{Co}^{\text{II}}\text{Cl}$. The two Co^{II} ions in **4a** are bridged by the two $\mu_{1,3}$ -Dipp- PO_2^- moieties of the two PO_2^- ligands through two O atoms of PO_2 unit [*syn-anti*-bridging mode; $\text{PO}_2\text{Co}^{\text{II}}_2$] displaying $\eta^1:\eta^1:\eta^1:\mu_2$ bridging mode by PO_2N donor set of the ligand. Each Co^{II} ion of **4a** is coordinated by one N atom of the $[(\text{Dipp})(\text{cAl})\text{P}^-]$ ligand, while two O atoms of this ligand acts as a *cis*-, *anti*-bridge between two Co^{II} ions. Finally, one terminal Cl atom completes the distorted tetrahedral geometry of each Co^{II} centre. The bond distances between Co1-O1/O2 are 1.941(2) Å, and 1.993(3) Å, respectively, where the former one is much shorter than the $\text{Co}_{\text{peripheral}}\text{-O}$ distance (1.9589(3) Å), whereas, the later one is comparable with the $\text{Co}_{\text{apex}}\text{-O}$ distance (2.036(2) Å) observed in **3a**. The P—C bond distances (1.843(4) Å) in **4a**, correspond to the typical P—C single bond [P—C bond distance in $\text{NHC}:\rightarrow\text{PCl}_3$ adduct is reported as 1.871(11) Å], and comparable to that of **3a** (1.8397(17) Å),²⁰ and slightly shorter than that of **2a** (1.8550(12) Å). The two P—O bond distances in **4a** are found to be almost identical (1.512(3) Å, 1.514(3) Å) representing the delocalization, which is also visible from the molecular orbitals in α -SOMO-58 and β -SOMO-52 (see ESI). These bond lengths are slightly longer than the P—O distances found in $\text{NHC}_2(\text{PO}_2)_2$ (1.470(2), 1.466(3) Å).²⁰ The distances between the two Co ions in **4a**, **4b** are found to be 4.247, 4.40 Å, respectively, which are significantly longer than that in **3a** (2.7046(4) Å).

The electron paramagnetic resonance (EPR) spectrum of **3a** in DCM at 77 K exhibited a broad signal presumably due to the distorted tetrahedral geometry of Co1 (side), and Co2 (central) ions. The broadening of the EPR signal can be rationalized by the positive D values (-14.4, +32.4 cm^{-1}), and the rhombic nature of the $\text{Co}(\text{II})$ ions (see ESI). The Mulliken spin density calculations (computed at UB3LYP-D3(BJ)/def2-TZVP level of theory) showed that the majority of the α -spin density of the model complex **3a'** (replacing Dipp groups by Me groups) is delocalized across the Co atoms (31.0%) located in the periphery, along with contributions from the central O atom (2.0%) and Cl atoms (1.2%) (Figure 3).

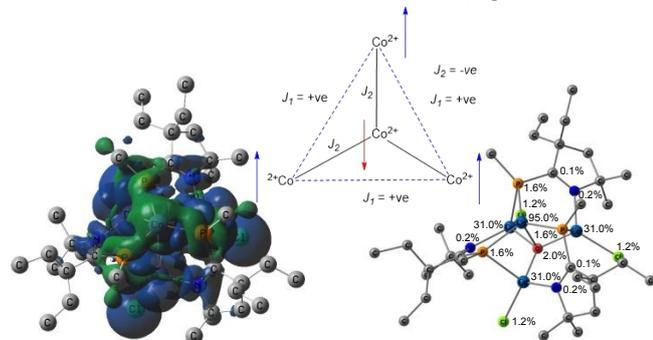


Figure 3. Mulliken α - (blue), β -spin (green) densities of the model complex $[(\text{Me})(\text{Et}_2\text{-cAl})\text{P}(\text{CoCl})_3\text{O}]$ (**3a'**) at $S = 3$ (computed at UB3LYP-D3(BJ)/def2-TZVP level of theory).

In contrast, the β -spin density is primarily distributed over the Co (axial) and P atoms, with the largest contribution coming from the Co atom (95.0%).

The temperature-dependent magnetic susceptibility measurements performed on **3a** within the temperature range of 2–300 K revealed that the experimentally observed χT susceptibility vs temperature values are slightly above the calculated molar Curie constant $C_{4\text{Co}(\text{II})} = 7.50 \text{ cm}^3 \text{ K mol}^{-1}$ (dashed line in Figure 4 (a)) for four free high spin Co^{II} ions, each with spin $S = 3/2$ within a formula unit (f.u.), and without any interactions between each other. The slightly increased value is ascribed to weak dominant ferromagnetic (FM) interaction as already indicated by the positive Weiss constant obtained from the Curie-Weiss fit (see ESI).

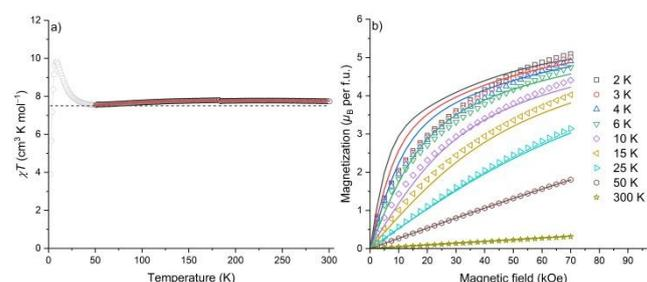


Figure 4. Experimental (open symbols), and simulated (solid lines) (a) χT vs T ; (b) magnetization vs magnetic field plots for **3a**. Dashed line in (a) represents the calculated molar Curie constant, $C_{4\text{Co}(\text{II})} = 7.50 \text{ cm}^3 \text{ K mol}^{-1}$ for four free Co^{II} ions, each with spin $S = 3/2$ per f.u.

For the magnetic model, a total spin $S = 3/2$ was ascribed to each Co site. The three Co1 (side) are exchange coupled via the isotropic exchange constant J_1 with each other, and each Co1 is coupled via J_2 to the central Co2 ion. Utilizing the program PH1²¹, isotropic exchange parameters were refined to $J_1 = 18.52(5) \text{ cm}^{-1}$, and $J_2 = -15.15(5) \text{ cm}^{-1}$, i.e. with a slightly dominant FM exchange interaction as also found by Curie-Weiss fit. Furthermore, the ZFS parameters (only the axial D parameter has been used for the applied model here) were refined to $D(\text{Co1}) = -14.4(1) \text{ cm}^{-1}$, and $D(\text{Co2}) = 32.4(1) \text{ cm}^{-1}$. The antiferromagnetic coupling between Co1 (side) and Co2 (central) creates a ground state with reduced magnetic moment due to the mutual partial cancelling out, and furthermore, the ZFS reduces the measured magnetization, especially, at low temperature due to the single-ion anisotropy that force the magnetic moments to be aligned along the statistically distributed (polycrystalline sample) uniaxial anisotropy axes (D).²² The spin ground state of previously reported $(\text{NHC})_4\text{Co}_4\text{S}_4$ cluster with Co—Co distances of $\sim 2.69 \text{ Å}$ was found to be $S = 3$ (see ESI).²³ The natural bond orbital (NBO) analysis performed on model complex **3a'** (calculated at UB3LYP/def2-TZVP level of theory) in septet state revealed that the α -SOMO corresponds to the delocalization of electrons on Co and O on the axial position, and P atoms on the periphery (Figure 5). The α -SOMO-1 corresponds to the 3-centered electron delocalization over $\text{Co}_{\text{periphery}}\text{-P-Co}_{\text{axial}}$ moiety, where the major coefficient resides on the p-orbital of P (75.6%). The



α -SOMO-5 corresponds to the σ -electron donation from O atom (83.5%) to the Co present at the axial position.

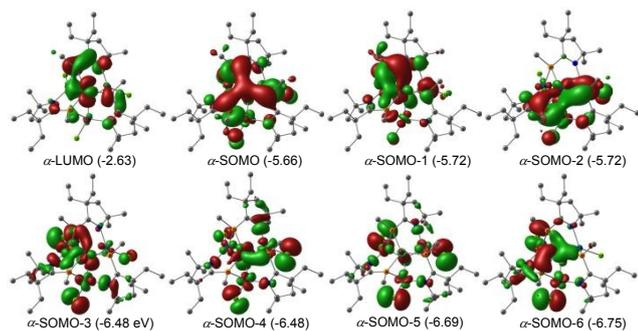


Figure 5. Selected Kohn-Sham orbitals of the model complex $[((\text{Me})(\text{Et}_2\text{cAl})\text{P}(\text{CoCl})_3)\text{O}]$ (**3a'**) at $S = 3$ (at UB3LYP-D3(BJ)/def2-TZVP level of theory; energies given in parentheses are in eV).

The EPR spectrum of **4a-4b** in DCM at 298 K exhibited the signal with a g_{eff} values of 2.0053, 2.0829, respectively (see **ESI**). The α -spin density of **4b** is predominantly found on the Co ions (45.6%), where the unpaired electron exists with only minimal contributions from O (0.69%, 0.62%), P (0.3%), and the ligand (C 0.1%; N 0.6%) (see **ESI**).

The DC magnetic susceptibility measurements of **4b** showed that the magnetic momentum per Co-ion is significantly higher than that of **3a** (see **ESI**). The χT product is $7.65 \text{ cm}^3 \text{ K mol}^{-1}$ at 300 K, which slowly decreases to $6.77 \text{ cm}^3 \text{ K mol}^{-1}$ at 28 K due to the spin-orbit-coupling of Co^{II} ions (see **ESI**).

In conclusion, we have developed a novel strategy for solid state isolation of the highly moisture, and oxygen-sensitive structurally well-defined Co^{II}_4 metal clusters, **3a-3b** with Co_4O core by reacting the Cs-salts **1a-1b** with anhydrous CoCl_2 at rt under argon atmosphere. The Mulliken spin density calculations on **3a'** revealed delocalized α -spin density across the peripheral Co ions with smaller contributions from central O, Cl atoms. **3a-3b** were successfully utilized for activation of aerial O_2 affording air-stable dimeric Co^{II} complexes **4a-4b**.

SR gratefully acknowledges STARS-IISC-MoE, (MoE-STARS/STARS-2/2023-0666), and IISER Tirupati for financial support. We acknowledge Subuhan Ahamed (IIT Madras) for generating the Hirshfeld plots, and EPR simulation.

Data availability

The data supporting this article (syntheses, UV-Vis, EPR, XPS, single-crystal X-ray data, magnetic data, computational details) are included as part of ESI.† Crystallographic data for **2a-2b**, **3a**, **4a-4b** have been deposited at CCDC (2324725 - 2324727, 2344451 - 2344452†), which can be obtained from <https://www.ccdc.cam.ac.uk/>.

Conflicts of interest

There are no conflicts to declare.

Notes and references

- (a) L. P. Battaglia, D. Delledonne, M. Nardelli, G. Predieri, G. P. Chiusoli, M. Costa and C. Pelizzi, *J. Organomet. Chem.*, 1998, **363**, 209. (b) C. Xia, K. Yang, S. G. Bott and M. G. Richmond, *Organometallics*, 1996, **15**, 4480. (c) M. Costa, G. Gervasio, D. Marabello and E. Sappa, *J. Organomet. Chem.*, 2002, **656**, 57. (d) F. Mafuné, Y. Wu, M. Yamaguchi and S. Kudoh, *J. Phys. Chem. A*, 2024, **128**, 3516.
- (a) L. Liu, Y. Su, J. Gao and J. Zhao, *Physica E*, 2012, **46**, 11. (b) T. Alonso-Lanza, A. Ayuela and F. Aguilera-Granja, *Chem. Phys. Chem.*, 2015, **16**, 3700. (c) K. García-Díez, J. Fernández-Fernández, J. A. Alonso and M. J. López, *Phys. Chem. Chem. Phys.*, 2018, **20**, 21163. (d) Y. Wang, L. Wang and S. Ma, *Appl. Surf. Sci.*, 2019, **481**, 1080.
- A. Han, W. Sun, X. Wan, D. Cai, X. Wang, F. Li, J. Shui and D. Wang, *Angew. Chem. Int. Ed.*, 2023, **62**, e202303185.
- K. García-Díez, J. Fernández-Fernández, J. A. Alonso and López, María J, *Phys. Chem. Chem. Phys.*, 2018, **20**, 21163.
- K. Chakarawat, P. C. Bunting and J. R. Long, *J. Am. Chem. Soc.*, 2018, **140**, 2058.
- J. Camacho-Bunquin, M. J. Ferguson and J. M. Stryker, *J. Am. Chem. Soc.*, 2013, **135**, 5537.
- Y. Luo, M. Li, Y. Dai, R. Zhao, F. Jiang, S. Wang and Y. Huang, *Inorg. Chem.*, 2021, **60**, 18251.
- (a) R. J. L. F. Aguilera-Granja, K. Michaelian and A. Vega, *Phys. Rev. B*, 2003, **67**, 174413. (b) F. Mafuné, Y. Wu, M. Yamaguchi and S. Kudoh, *J. Phys. Chem. A*, 2024, **128**, 3516. (c) S. Lee, A. Halder, G. A. Ferguson, S. Seifert, R. E. Winans, D. Teschner, R. Schlögl, V. Papaefthimiou, J. Greeley, L. A. Curtiss and S. Vajda, *Nat. Commun.*, 2019, **10**, 954.
- J. Facio-Muñoz, D. Hernández-Velázquez, G. Guzmán-Ramírez, R. Flores-Moreno, J. Rodríguez-Zavala and F. Tenorio, *J. Mol. Model.*, 2022, **28**, 197.
- X. Xie, M. Zhu, F. Xiao, Y. Xiang, H. Zhong, Z. Ao and H. Huang, *JACS Au*, 2023, **3**, 1496.
- W. Deng, D. He, D. Chen, Z. Huang, J. Deng and Y. Luo, *Commun. Mater.*, 2024, **5**, 215.
- E. Nag, M. Francis, D. Putta and S. Roy, *Chem. Eur. J.*, 2023, e202302120.
- Y. Wang, Y. Xie, P. Wie, H. F. Schaefer III, P.v.R. Schleyer and G. H. Robinson, *J. Am. Chem. Soc.*, 2013, **135**, 19139.
- J. Abbenseth, F. Wätjen, M. Finger and S. Schneider, *Angew. Chem. Int. Ed.*, 2020, **59**, 23574.
- S. J. Hunter, K.W. Hipps and A. H. Francis, *Chem. Phys.*, 1979, **39**, 209.
- K. Pal, O. B. Hemming, B. M. Day, T. Pugh, D. J. Evans and R. A. Layfield, *Angew. Chem. Int. Ed.*, 2016, **55**, 1690.
- J. Kumar, N. V. T. S. M. Gorantla, S. Roy, A. N. Paesch, R. Herbst-Irmer, D. Stalke, C. Anusha, S. De, P. Parameswaran and H. W. Roesky, K. C. Mondal, *ChemistrySelect*, 2018, **3**, 8221.
- K. C. Mondal, P. P. Samuel, H. W. Roesky, E. Carl, R. Herbst-Irmer, D. Stalke, B. Schwederski, W. Kaim, L. Ungur, L. F. Chibotaru, M. Hermann and G. Frenking, *J. Am. Chem. Soc.*, 2014, **136**, 1770.
- R. Weller, A. Gonzalez, H. Gottschling, von Hänisch and W. C. Gunnar, *Z. Anorg. Allg. Chem.*, 2022, **648**, e202100338.
- Y. Wang, Y. Xie, M. Y. Abraham, R. J. Jr, P. Wei, H. F. III, Paul and G. H. Robinson, *Organometallics*, 2010, **29**, 4778.
- N. F. Chilton, R. P. Anderson, L. D. Turner, A. Soncini and K. S. Murray *J. Comput. Chem.*, 2013, **34**, 1164.
- B. Schwarz, and Q. Fu, *Eur. J. Inorg. Chem.*, 2024, **2024**, e202400162.
- L. Deng, E. Bill, K. Wieghardt and R. H. Holm, *J. Am. Chem. Soc.*, 2009, **131**, 11213.



Data availability

The data supporting this article (Experimental details, UV-vis, IR, EPR, and NMR spectroscopic data, CV data, single-crystal X-ray data, computational details, data for magnetic measurements) have been included as part of the ESI. †Crystallographic data for **2a-2b**, **3a**, **4a-4b** have been deposited at the CCDC (2324725 2344451 2324727 2324726 2344452†), and can be obtained from <https://www.ccdc.cam.ac.uk/>.

